PCCP

PAPER

View Article Online
View Journal | View Issue

Cite this: *Phys. Chem. Chem. Phys.*, 2015, **17**, 32328

Efficient surface enhanced Raman scattering on confeito-like gold nanoparticle-adsorbed self-assembled monolayers†

Chia-Chi Chang,[a] Toyoko Imae,*[ab] Liang-Yih Chen*[a] and Masaki Ujihara[b]

Received 14th September 2015,
Accepted 2nd November 2015

DOI: 10.1039/c5cp05490g

www.rsc.org/pccp

Confeito-like gold nanoparticles (AuNPs; average diameter = 80 nm) exhibiting a plasmon absorption band at 590 nm were adsorbed through immersion-adsorption on two self-assembled monolayers (SAMs) of 3-aminopropyltriethoxysilane (APTES-SAM) and polystyrene spheres coated with amine-terminated poly(amido amine) dendrimers (DEN/PS-SAM). The surface enhanced Raman scattering (SERS) effect on the SAM substrates was examined using the molecules of a probe dye, rhodamine 6G (R6G). The Raman scattering was strongly intensified on both substrates, but the enhancement factor (>10 000) of the AuNP/DEN/PS-SAM hierarchy substrate was 5–10 times higher than that of the AuNP/APTES-SAM substrate. This strong enhancement is attributed to the large surface area of the substrate and the presence of hot spots. Furthermore, analyzing the R6G concentration dependence of SERS suggested that the enhancement mechanism effectively excited the R6G molecules in the first layer on the hot spots and invoked the strong SERS effect. These results indicate that the SERS activity of confeito-like AuNPs on SAM substrates has high potential in molecular electronic devices and ultrasensitive analyses.

Introduction

Metal nanoparticles are some of the most crucial materials in nanotechnology, because they possess unique physical (electronic, magnetic, and optical) and chemical (structural, catalytic, and sensing) properties, which differ substantially from those of the bulk materials.[1] Because such properties profoundly depend on the particle size and shape,[2,3] the synthesis and characterization of metal nanoparticles have attracted considerable attention both academically and industrially.[4] For instance, sphere-, rod-, plate- flower- and confeito-like gold nanoparticles (AuNPs) have been synthesized.[5–7] Among the properties of metal nanoparticles, the resonance between an electromagnetic field and a localized surface plasmon wave at the surface of the metal particles creates a plasmon electromagnetic field and causes surface plasmon enhancement or resonance.[8–11] Surface plasmon works on infrared (IR) absorption,[12–14] Raman scattering[15–18] and fluorescence;[19,20] however, most studies have focused on the qualitative surface enhanced properties.

Many studies have focused on assembling structures with a high-ordered arrangement of metal nanoparticles,[5,21] because a dense metal nanoparticle arrangement facilitates electron transport and possesses optical properties.[22] Nanoparticle assemblies can be prepared through many methods, including chemisorption deposition,[23] electrostatic deposition,[24] electrochemical deposition,[25] electrophoretic deposition,[26] chemical vapor deposition (CVD),[27] and Langmuir–Blodgett deposition.[28] Electrostatic deposition is easy because of the spontaneous reaction and the short deposition time and is suitable for precisely controlling nanoparticles at interfaces; thus, it has several advantages over the other methods. In addition, this procedure is independent of the nanoparticle shape and size, because its principle is based on the attractive force between positive and negative charges.

In this study, two types of SERS-active self-assembled monolayers (SAMs) were fabricated using confeito-like AuNPs:[29] one was prepared using 3-aminopropyltriethoxysilane (APTES-SAM) and another was on the SAM of anionic polystyrene (PS) spheres coated with amine-terminated poly(amido amine) (PAMAM) dendrimers (DEN/PS-SAM). Since both SAMs possess cationic (amine) surfaces, anionic (carboxylate charged) confeito-like AuNPs can electrostatically adsorb on these SAMs. Since the patterned DEN/PS-SAM may have a larger surface area than the

[a] *Department of Chemical Engineering, National Taiwan University of Science and Technology, 43 Section 4, Keelung Road, Taipei 10607, Taiwan, Republic of China. E-mail: imae@mail.ntust.edu.tw, sampraslyc@gmail.com; Fax: +886 2 27303627; Tel: +886 2 27303627*

[b] *Graduate Institute of Applied Science and Technology, National Taiwan University of Science and Technology, 43 Section 4, Keelung Road, Taipei 10607, Taiwan, Republic of China*

† Electronic supplementary information (ESI) available. See DOI: 10.1039/c5cp05490g

flat APTES-SAM, the DEN/PS-SAM can be expected to be adsorbed with a large amount of AuNPs. Confeito-like AuNP-deposited SAM substrates, instead of the conventional spherical CVD AuNP films, were used for investigating surface enhanced Raman scattering (SERS), because confeito-like AuNPs exhibit a strong and broad plasmon band in the near-infrared region.[29] The efficiency of SERS was quantitatively evaluated by calculating the enhancement factor, for demonstrating the considerable enhancement of SERS of the confeito-like AuNPs deposited on SAM substrates and for elucidating the contributing factors toward the SERS effect. Surface enhanced infrared absorption spectroscopic investigation was performed previously using confeito-like AuNPs.[30] However, this is the first application of confeito-like AuNPs to SERS.

Experimental section

Reagents and materials

Citric acid (anhydrous), 3-aminopropyl-triethoxysilane (99%, APTES), rhodamine 6G (99%, R6G) and hydrogen peroxide (35 wt% in water) were purchased from Acros Organics. An amine-terminated poly(amido amine) dendrimer (ethylenediamine core, generation 4.0 (G4), 10 wt% in methanol) and sodium tetrachloroaurate(III) dihydrate were purchased from Sigma-Aldrich. A polystyrene sphere (500 nm in diameter) was purchased from Alfa Aesar and sodium dodecyl sulfate (SDS) was purchased from J. T. Baker. Phosphate buffer powder (1/15 M, pH 7.4, PB) was purchased from Wako Chemicals. Other reagents were of commercial grades and all reagents were used without further purification. Ultrapure water (resistivity: 18.2 MΩ cm) was obtained from a Yamato Millipore WT100. ITO glass (1×1 cm^2 piece) (sheet resistance: 25 Ω square^{-1}, AimCore Technology), which was cleaned by sonicating in a detergent solution, acetone, isopropanol and water, was hydroxylated in a piranha solution (a mixture (3 : 1 v/v) of H_2SO_4 and H_2O_2), rinsed with water, and then dried under N_2 gas.

Confeito-like AuNPs were synthesized as previously reported.[29] Briefly, for the mixture of sodium tetrachloroaurate(III) (4 ml, 1 mM) and citric acid (5.8 mole), hydrogen peroxide (180 μl) and subsequently sodium hydroxide (8 ml, 0.1 mM) were added under stirring. The aqueous solution was kept overnight to complete the reaction and to decompose excess hydrogen peroxide, and finally a blue dispersion of confeito-like AuNPs was obtained. After the dispersion (Au: 0.1 mM) was centrifuged at 2100 rpm for 15 min, the precipitates were rinsed with water three times and dispersed in water to obtain the dispersions of highly concentrated confeito-like AuNPs.

Deposition of confeito-like AuNPs on amine-surface substrates

Patterned APTES-SAM, and unpatterned APTES-SAM and DEN/PS-SAM substrates were prepared as follows. The APTES-SAM substrate was obtained by immersing the cleaned ITO glass overnight in an ethanol solution of 2 wt% APTES at room temperature to form a silane monolayer.[31] Then the APTES-SAM on glass was rinsed with ethanol several times and then heated overnight at 110 °C to remove residual solvent and achieve the chemisorption of the SAM. The SAM substrate was exposed for 2 h to UV light (172 nm) in nitrogen gas through a photomask to prepare a patterned SAM substrate.[31]

A uniform self-assembled monolayer of PS spheres was prepared by immersing the ITO glass into an aqueous dispersion of the PS sphere (10 wt%), to which sodium dodecyl sulfate (2 wt%) was added as a dispersion agent.[27,32–34] Then, PS-SAM on glass was held for 30 min at 80 °C and 150 s at 100 °C, so that the adhesion of the PS sphere on glass becomes more stable. The PS-SAM substrate was immersed into an aqueous solution of the G4-PAMAM dendrimer (DEN) (0.1 wt%) for 30 min, rinsed three times with phosphate buffer saline at pH 7.4, where 0.175 g of NaCl was dissolved in 20 ml of buffer saline.

The adhesion of confeito-like AuNPs on (both patterned and unpatterned) APTES-SAM and DEN/PS-SAM was performed by immersing the substrates in aqueous dispersions of confeito-like AuNPs (1, 5 and 10 mM) for 30 min at pH 6.3 for APTES-SAM and at pH 11.2 for DEN/PS-SAM, rinsing with water three times and drying at room temperature. Then the aqueous R6G solutions (20 μl) at various concentrations (from 1 μM to 1 mM) were dropped on the substrates and the substrates were dried. These specimens were utilized for substrate characterization and SERS measurements.

Instruments

An ultraviolet-visible absorption spectrophotometer (UV-VIS, V-670, JASCO) was operated at a scan speed of 200 nm min^{-1}. Infrared (IR) absorption spectra were obtained on a FTIR spectrophotometer (Thermo scientific, Nicolet 6700) with an accumulation of 64 times. Transmission electron microscopy (TEM) images were taken using a Hitachi H-7000 instrument, operated at 100 kV. The particle size and zeta potential were measured by dynamic light scattering (DLS, SZ-100, HORIBA scientific). Patterned SAMs were prepared by photolithography with an excimer lamp (Ushio Electric UER20-172V, λ = 172 nm with a power density of 10 mW cm^{-2}).[31] X-ray photoelectron spectroscopic (XPS) spectra were obtained on a theta probe ESCA VG Scientific, using a monochromatic AlKα source at a pressure of 2×10^{-9} mbar. A scanning electron microscope (SEM, JSM-6390) was operated at an accelerating voltage of 15 kV. SERS spectra were acquired using a Raman scattering spectrometer (BWII-UniRam) with 21 of 0.54 mW power at 532 nm excitation and a focused laser spot of a 1 μm diameter. The exposure and accumulation were 1 s and 30 times, respectively.

Results and discussion

Characterization of confeito-like AuNPs on APTES-SAM and DEN/PS-SAM substrates

Confeito-like AuNPs were synthesized by reducing trivalent Au ions by using hydrogen peroxide as the reductant and citric acid as the capping agent in an alkaline solution, according to the green chemistry approach.[29] The characterization is presented in the ESI,† (Fig. S1–S8). The confeito-like AuNPs were

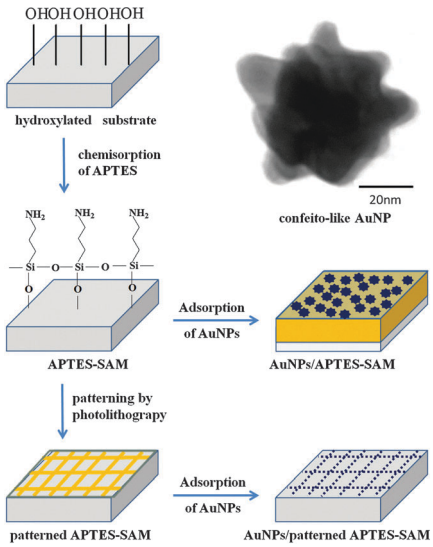

Scheme 1 Schematic illustration of adsorption of confeito-like AuNPs on the APTES-SAM substrate.

stably dispersed in water because they were coated with citrate. The AuNPs had an average diameter of 80 nm (inset, Scheme 1) and a plasmon absorption band at 590 nm (Fig. S2, ESI†). These AuNPs were adsorbed through immersion-adsorption on two amine-terminated SAM substrates, APTES-SAM and DEN/PS-SAM, and were prepared using Schemes 1 and 2, respectively, as described in the Experimental section.

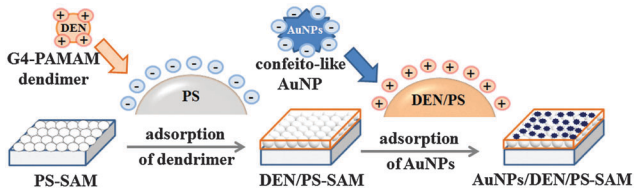

Scheme 2 Schematic illustration of adsorption of confeito-like AuNPs on the DEN/PS-SAM hierarchy substrate.

The APTES-SAM substrate was chemically analyzed through XPS. O1s, N1s, C1s, Si2s, and Si2p peaks in Fig. S9 (ESI†) were indicative of APTES. Deconvolution of each peak (Fig. 1) showed that the binding energy of the N1s peak was attributed mainly to protonated amine (403.6 eV),[35,36] and that of the C1s peak was attributed to the two components of C–O + C–N + C–Si (286.6 eV) and C–O–Si (287.9 eV) bonds. The O1s peak included O–Si, Si–O–Si and O–C bonds at 532.7, 533.6 and 534.6 eV, respectively, and the Si2p peak indicated the binding energy (104.44 eV) of Si–O–Si + Si–O after the hydrolysis of the ethoxy group in APTES.[31,37–39] Thus, the successful formation of APTES-SAM was confirmed from XPS.

The adsorption behavior of the confeito-like AuNPs on substrates was first examined on two SAM substrates: APTES-SAM and UV-irradiated APTES-SAM. In the SEM images presented in Fig. 2, many small spots were visually detected on APTES-SAM (Fig. 2(a)), but no spots were detected on the UV-irradiated APTES-SAM (Fig. 2(b)). A similar phenomenon was confirmed on the patterned APTES-SAM substrate (Fig. 2(c)). The spots were observed only in the non-irradiated frame pattern region but not in the irradiated rectangular pattern region. Energy dispersive spectroscopy was used for analyzing the composition of the spot masked by the circle in Fig. 2(c), and the result is shown in Fig. 2(d). The presence of Au peaks indicated that the spots were those of the confeito-like AuNPs. Thus, the aforementioned findings confirmed that the confeito-like AuNPs were selectively adsorbed on the APTES-SAM.

The APTES-SAM surface was terminated using the amino groups of APTES,[31] and the confeito-like AuNP surface possessed carboxylate groups from a protecting agent (citric acid).[29] Therefore, the confeito-like AuNPs adsorbed on the APTES-SAM substrate because of electrostatic attraction between the amine and

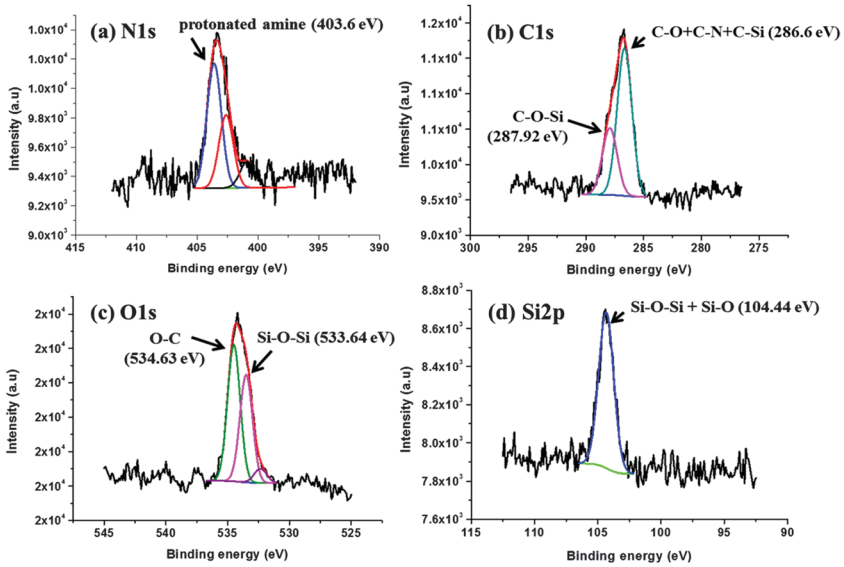

Fig. 1 XPS spectra of APTES-SAM. (a) N1s, (b) C1s, (c) O1s and (d) Si2p.

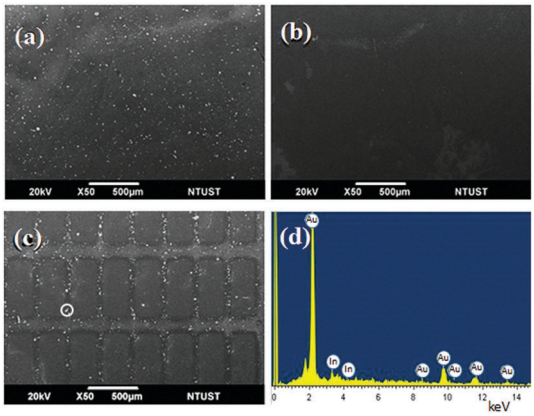

Fig. 2 SEM images of confeito-like AuNPs adsorbed on the APTES-SAM substrates (a) before and (b) after UV-irradiation, and (c) on the patterned APTES-SAM substrate. The scale bar indicates 500 μm. (d) An EDX spectrum of confeito-like AuNPs in the 1 μm diameter area marked on the patterned APTES-SAM substrate (c).

carboxylate groups. However, the AuNPs did not adsorb on the UV-irradiated APTES-SAM because the surface of the UV-treated APTES-SAM was altered nonreactive to confeito-like AuNPs.

The confeito-like AuNPs were adsorbed on the APTES-SAM substrates through dispersions of different AuNP concentrations (Au: 1, 5, and 10 mM), and their SEM images are compared in Fig. 3. The surface density of AuNPs on the APTES-SAM substrates was altered by changing the AuNP concentrations. At high AuNP concentrations, the substrate surface was densely covered by the AuNPs. At AuNP concentrations of 1 and 5 mM, the AuNPs were uniformly distributed on the APTES-SAM substrates. Such a configuration could be attributed to the relatively well-ordered arrangement of APTES-SAM and the strong interaction between APTES-SAM and the AuNPs caused by the high charge density of dense amine terminals on the substrate. However, at a high AuNP concentration (*e.g.* 10 mM), the confeito-like AuNPs aggregated with an island-like texture on the APTES-SAM substrates, indicating the accumulation of AuNPs.

In a previous study, an ordered monolayer of PSs over a large area was successfully obtained through a self-assembling deposition,[27] where the diameter of the PS was 500 nm. Successively, the surfaces of PSs were coated with amine-terminated PAMAM dendrimers and adsorbed with confeito-like AuNPs (Scheme 2). Fig. 4 shows the SEM images of the DEN/PS-SAM and AuNP/DEN/PS-SAM substrates. Surface modification can be elucidated from the disappearance of the smoothness of the PS surface after the adsorption of confeito-like AuNPs on DEN/PS-SAM. The surface of PS-SAM is negatively charged because anionic sodium dodecyl sulfate surrounds the surface, indicating that cationic PAMAM dendrimers play a major role in the adsorption of anionic confeito-like AuNPs through electrostatic attraction. Thus, strong interactions, including van der Waals, capillary force (induced by the PS array) and electrostatic attractions, promote this layer-by-layer self-assembly on the substrate. The slight roughness on DEN/PS-SAM should be adequate to trap the bosses (tips) of confeito-like Au nanoparticles. As a result of dense adsorption of AuNPs on DEN/PS-SAM, only bosses (tips) of AuNPs are observed (see Fig. 4(c)) but no independent AuNPs are on the DEN/PS-SAM surface.

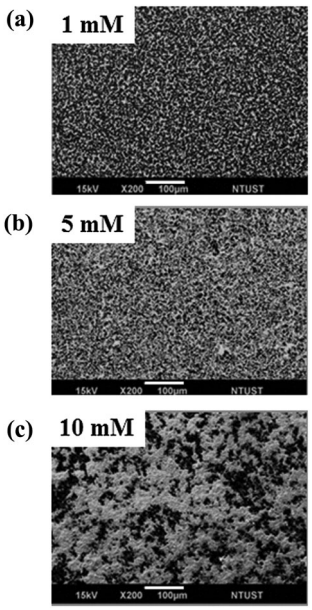

Fig. 3 SEM images of confeito-like AuNPs on APTES-SAM substrates prepared from different concentrations of AuNP dispersions. Au concentration: (a) 1 mM, (b) 5 mM and (c) 10 mM. The scale bar indicates 100 μm.

SERS on AuNP/APTES-SAM and AuNP/DEN/PS-SAM substrates

AuNP/APTES-SAM and AuNP/DEN/PS-SAM substrates were used for confirming SERS activities by using an organic dye, rhodamine 6G (R6G) (Fig. S10, ESI†). The negative charge of citric acid coating on AuNPs helped the AuNPs bind with the positively charged R6G within the plasmon electromagnetic field provided in

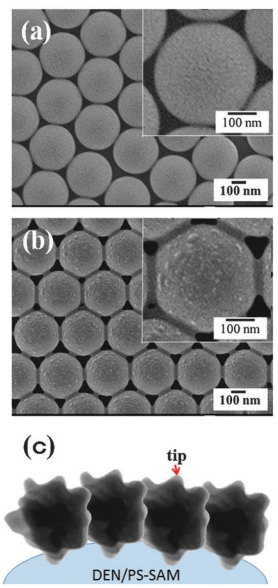

Fig. 4 SEM images of (a) DEN/PS-SAM and (b) AuNP/DEN/PS-SAM substrates and (c) schematic illustration of AuNP/DEN/PS-SAM substrates.

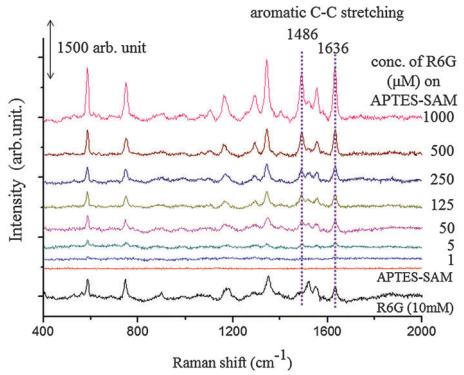

Fig. 5 SERS spectra of R6G at various concentrations on the confeito-like AuNP/APTES-SAM substrate. The substrate was prepared from a dispersion of confeito-like AuNPs at 5 mM.

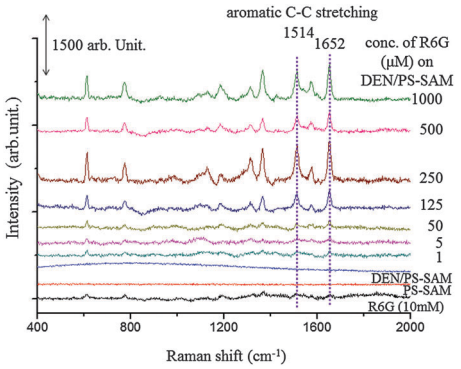

Fig. 6 SERS spectra of R6G at various concentrations on the confeito-like AuNP/DEN/PS-SAM substrate. The substrate was prepared from a dispersion of confeito-like AuNPs at 5 mM.

proximity to the AuNPs. Fig. 5 shows the Raman spectra of the AuNP/APTES-SAM substrate prepared with 5 mM of confeito-like AuNPs. When the spectra were compared with the spectrum of an APTES-SAM substrate without AuNPs, the SERS effect was clearly observed. In addition, even at a low R6G concentration (5 μM), the spectrum displayed clear Raman bands of R6G at 587, 746, 1164, 1297, 1343, 1486, 1555 and 1636 cm^{-1}, consistent with those of R6G (10 mM) on a substrate without AuNP/APTES-SAM.[22,40]

The intensities of the Raman bands of R6G decreased as the R6G concentration was decreased, and the bands were barely detectable at an R6G concentration of 1 μM (Fig. 5). Similar results were obtained, when AuNP/APTES-SAM substrates were prepared using AuNP concentrations of 1 and 10 mM (Fig. S11 and S12, ESI†). However, at a high AuNP concentration (10 mM), the Raman intensity was adequate even at a low R6G concentration (1 μM). This finding may be attributed to the high AuNP density observed from SEM images (Fig. 3), increasing the number of SERS active sites (hot spots). These hot spots, one of the primary contributing factors toward the SERS effect, are formed at junctions among metal nanoparticles.[41,42] A large number of junctions can produce a stronger plasmon electromagnetic field.

Fig. 6, Fig. S13 and S14 (ESI†) show the Raman spectra obtained after R6G was deposited on AuNP/DEN/PS-SAM substrates prepared using confeito-like AuNPs at concentrations of 1, 5 and 10 mM. Raman bands of R6G were observed at 610, 773, 1184, 1314, 1366, 1514, 1574, and 1652 cm^{-1}. These bands were nearly consistent with the spectral profiles of R6G on AuNP/APTES-SAM substrates (Fig. 5, Fig. S11 and S12, ESI†). When R6G molecules were deposited on the AuNP surface as a monolayer, they were directly enhanced by the surface plasmon wave and moreover by the hot spots on AuNP/DEN/PS-SAM. However, when the concentration of R6G was high, R6G molecules accumulated to form a thick layer. Compared with the R6G monolayer on AuNPs, the effects of the surface plasmon wave and hot spots were less for the accumulated R6G layer because the accumulated molecules were away from the AuNP surface. Moreover, the thick R6G layer on AuNPs absorbed the excitation light; consequently, the apparent surface enhancement effect was diminished. With regard to the AuNP/APTES-SAM substrate, the accumulation of R6G was not distinct even at a high R6G concentration.

Evaluation of enhancement factors (EFs)

Enhancement factors (EFs) were investigated for quantifying the potential uses of confeito-like AuNPs for SERS analysis. EFs were evaluated using the Raman bands of aromatic C–C stretching vibration modes of R6G observed at 1486 and 1636 cm^{-1} on the APTES-SAM substrate and at 1514 and 1652 cm^{-1} on the DEN/PS-SAM substrate. EFs were evaluated using the following equation.[43]

$$\mathrm{EF} = \left(\frac{I_{\mathrm{SERS}}}{I_{\mathrm{Raman}}}\right) \times \left(\frac{C_{\mathrm{Raman}}}{C_{\mathrm{SERS}}}\right) \quad (1)$$

where I_{SERS} and I_{Raman} are the intensities of a corresponding Raman band of R6G on substrates with and without AuNP/APTES-SAM or AuNP/DEN/PS-SAM, respectively. C_{SERS} and C_{Raman} are the concentrations of R6G on substrates with and without AuNP/APTES-SAM or AuNP/DEN/PS-SAM, respectively.

For both substrates, EFs were calculated using data in Fig. 5 and 6 and Fig. S11–S14 (ESI†) and plotted in Fig. 7. Although the results displayed a similar trend, SERS activity was stronger on the AuNP/DEN/PS-SAM substrate than on the AuNP/APTES-SAM substrate, because the EFs of the AuNP/DEN/PS-SAM substrate were 5–10-times larger than those of the AuNP/APTES-SAM substrate. A larger number of active sites for SERS were possibly created on the AuNP/DEN/PS-SAM surface than on the AuNP/APTES-SAM surface, because the DEN/PS-SAM holds a larger amount of AuNPs on its surface than the APTES-SAM does, as illustrated in Fig. 4(c). Incidentally, the total surface area of the PS-SAM substrate was approximately 3.14-times larger than that of the flat APTES-SAM substrate, because the surface of the PS-SAM substrate comprised an array of PS spheres. Thus, the number of hot spots was larger on AuNP/DEN/PS-SAM because of the ordered arrangement of PSs.

For describing the adsorption behavior of R6G on the hot spots, the Freundlich equation (eqn (2)) can be empirically used.

$$\frac{x}{m} = KC_{\mathrm{SERS}}^{1/n} \quad (2)$$

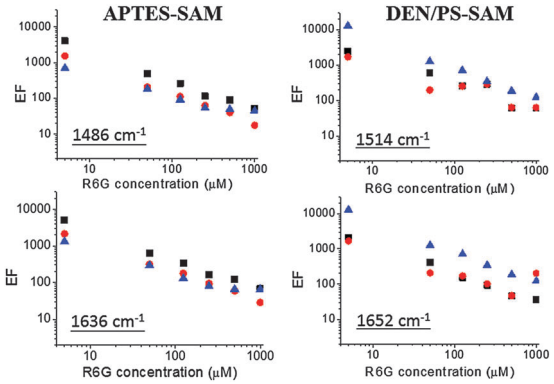

Fig. 7 Log–log plots of enhancement factors against the concentration of R6G on AuNP/APTES-SAM and AuNP/DEN/PS-SAM substrates. The concentration of AuNPs for the preparation of the substrate: ▲ 1 mM, ● 5 mM and ■ 10 mM. The inset wavenumbers denote the target Raman bands.

where x and m indicate the mass of the adsorbate and the adsorbent, respectively. K and n are empirical constants obtained from the data. Suppose I_{SERS} is proportional to x/m with a proportional constant, A, then EF in eqn (1) will be as follows:

$$\mathrm{EF} = AB\frac{x/m}{C_{\mathrm{SERS}}} \tag{3}$$

where B is a constant representing $C_{\mathrm{Raman}}/I_{\mathrm{Raman}}$. Then, eqn (2) and (3) are merged into eqn (4) or (5).

$$\mathrm{EF} = ABKC_{\mathrm{SERS}}^{\left(\frac{1}{n}-1\right)} \tag{4}$$

$$\log \mathrm{EF} = \left(\frac{1}{n}-1\right)\log C_{\mathrm{SERS}} + \log ABK \tag{5}$$

The log–log plots of EFs against R6G concentration decreased almost linearly (Fig. 7). This linearity suggested that I_{SERS} was proportional to the adsorbed amount of R6G on hot spots as assumed above. If not, the proportional constant A decreased as the adsorption amount increased. Our first assumption implied that the surface-enhancement effect on R6G is constant for all concentrations, whereas the adsorption amount of R6G followed the Freundlich equation. Our second assumption implied that the hot spots were already saturated at a low concentration and the surface-enhancement effect decreased as the distance increased. The R6G molecules in the first layer on the hot spots are effectively excited and invoke the strong SERS, and the additional molecules, accumulated in multilayers, caused less enhancement. Upon considering the high concentration of R6G, the second assumption seems to be rational.

The highest EFs were provided, when 10 mM of AuNPs was used for preparing the AuNP/APTES-SAM substrate; however, the highest EFs were obtained, when 1 mM of AuNPs was used for preparing the AuNP/DEN/PS-SAM substrate, suggesting that a large number of AuNPs causes a more number of hot spots on the APTES-SAM substrate and the dense accumulation of AuNPs may inhibit the formation of hot spots on the DEN/PS-SAM substrate. Therefore, the amount of AuNPs on the substrate must be optimized using an AuNP concentration for generating a high surface plasmon electromagnetic field on AuNPs.

EFs of more than 4 orders were obtained on an AuNP/DEN/PS-SAM substrate prepared using 1 mM of AuNPs. This finding indicates that the AuNP/DEN/PS-SAM substrate was superior to the AuNP/APTES-SAM substrate, which attained the highest EF of several thousands at an AuNP concentration of 10 mM. Meanwhile, the substrate with confeito-like AuNPs was used for surface-enhanced infrared absorption spectra (SEIRAS) and EFs of several hundreds were achieved, which were considerably high compared with those of other SEIRAS substrates.[44] Thus, because of their unique morphology the confeito-like AuNPs can be preferably used for both SERS and SEIRAS.

Conclusions

Confeito-like AuNPs synthesized using green chemistry[29] have wide plasmon absorption bands expanded in the near-visible region. The confeito-like AuNPs were successfully adsorbed on the APTES-SAM and DEN/PS-SAM substrates with amine-terminated surfaces because these AuNPs, coated with citric acid, strongly interacted with amine-terminated surfaces mainly because of electrostatic attraction.

Subsequently, the surface-enhancement effects of confeito-like AuNPs on these substrates were investigated using R6G as the analyte. The Raman band intensities of R6G on AuNP/DEN/PS-SAM and AuNP/APTES-SAM substrates were considerably higher than those of R6G on substrates without SAMs, suggesting that the confeito-like AuNPs caused the prominent SERS effect: the surface-enhancement effect on the AuNP/DEN/PS-SAM substrate was more than 10 000 times and the AuNP/APTES-SAM substrate exhibited the maximum effect of several thousand times. The characteristics of the AuNP/DEN/PS-SAM substrate can be associated with the large surface area of PS-SAM. In addition, the abundant active sites (hot spots) among closely arranged AuNPs on the close-packed PS array can enlarge the surface-enhancement effect.

On the concentration dependencies of SERS, their linear correlations in log–log plots indicated Freundlich type adsorption behaviors. This information is useful for designing plasmonic devices for quantitative analyses in various applications. Thus, because of their unique plasmonic properties, the confeito-like AuNPs and the nanoassemblies including these AuNPs were shown to possess high potential for use in molecular electronic devices and ultrasensitive chemical and biomedical analyses and sensing.

Acknowledgements

The part of this research was financially supported by the Research fund (104H4509) of National Taiwan University of Science and Technology.

References

1 G. Schmid, *Nanoparticles: From Theory to Application*, John Wiley & Sons, 2010.
2 S. Link and M. A. El-Sayed, *J. Phys. Chem. B*, 1999, **103**, 4212–4217.
3 M. Li, S. K. Cushing, J. Zhang, J. Lankford, Z. P. Aguilar, D. Ma and N. Wu, *Nanotechnology*, 2012, **23**, 115501.
4 T. K. Sau, A. L. Rogach, F. Jäckel, T. A. Klar and J. Feldmann, *Adv. Mater.*, 2010, **22**, 1805–1825.
5 K. Mitamura, T. Imae, N. Saito and O. Takai, *J. Phys. Chem. B*, 2007, **111**, 8891–8898.
6 J. Sharma, Y. Tai and T. Imae, *J. Phys. Chem. C*, 2008, **112**, 17033–17037.
7 L. Wang, C.-H. Liu, Y. Nemoto, N. Fukata, K. C.-W. Wu and Y. Yamauchi, *RSC Adv.*, 2012, **2**, 4608–4611.
8 M. Fleischmann, P. J. Hendra and A. McQuillan, *Chem. Phys. Lett.*, 1974, **26**, 163–166.
9 M. G. Albrecht and J. A. Creighton, *J. Am. Chem. Soc.*, 1977, **99**, 5215–5217.
10 D. L. Jeanmaire and R. P. Van Duyne, *J. Electroanal. Chem.*, 1977, **84**, 1–20.
11 Z. Zhang and T. Imae, *J. Colloid Interface Sci.*, 2001, **233**, 99–106.
12 T. Imae and H. Torii, *J. Phys. Chem. B*, 2000, **104**, 9218–9224.
13 Z. Zhang and T. Imae, *Nano Lett.*, 2001, **1**, 241–243.
14 M. Ito, T. Imae, K. Aoi, K. Tsutsumiuchi, H. Noda and M. Okada, *Langmuir*, 2002, **18**, 9757–9764.
15 A. Mal'Shukov, *Phys. Rep.*, 1990, **194**, 343–349.
16 Z. Zhang, T. Imae, H. Sato, A. Watanabe and Y. Ozaki, *Langmuir*, 2001, **17**, 4564–4568.
17 C. E. Talley, J. B. Jackson, C. Oubre, N. K. Grady, C. W. Hollars, S. M. Lane, T. R. Huser, P. Nordlander and N. J. Halas, *Nano Lett.*, 2005, **5**, 1569–1574.
18 K. Kim, K. L. Kim and S. J. Lee, *Chem. Phys. Lett.*, 2005, **403**, 77–82.
19 K. Mitamura, T. Imae, S. Tian and W. Knoll, *Langmuir*, 2008, **24**, 2266–2270.
20 K.-I. Yoshida, T. Itoh, V. Biju, M. Ishikawa and Y. Ozaki, *Phys. Rev. B: Condens. Matter Mater. Phys.*, 2009, **79**, 085419.
21 X. Zhang and T. Imae, *J. Phys. Chem. C*, 2009, **113**, 5947–5951.
22 T. Imae and X. Zhang, *J. Taiwan Inst. Chem. Eng.*, 2014, **45**, 3081–3084.
23 M. Fan and A. G. Brolo, *ChemPhysChem*, 2008, **9**, 1899–1907.
24 J. Lee, B. Hua, S. Park, M. Ha, Y. Lee, Z. Fan and H. Ko, *Nanoscale*, 2014, **6**, 616–623.
25 G. Duan, W. Cai, Y. Luo, Y. Li and Y. Lei, *Appl. Phys. Lett.*, 2006, **89**, 181918.
26 H.-W. Chen, C.-Y. Nong, C.-W. King, C.-Y. Mou, K. C.-W. Wu and K.-C. Ho, *J. Power Sources*, 2015, **288**, 221–228.
27 C. L. Haynes and R. P. Van Duyne, *J. Phys. Chem. B*, 2001, **105**, 5599–5611.
28 V. Santhanam, J. Liu, R. Agarwal and R. P. Andres, *Langmuir*, 2003, **19**, 7881–7887.
29 M. Ujihara and T. Imae, *Colloids Surf., A*, 2013, **436**, 380–385.
30 M. Ujihara, N. M. Dang, C.-C. Chang and T. Imae, *J. Taiwan Inst. Chem. Eng.*, 2014, **45**, 3085–3089.
31 P. D. Adhikari, T. Imae and S. Motojima, *Chem. Eng. J.*, 2011, **174**, 693–698.
32 J. Rybczynski, U. Ebels and M. Giersig, *Colloids Surf., A*, 2003, **219**, 1–6.
33 X. Wang, C. J. Summers and Z. L. Wang, *Nano Lett.*, 2004, **4**, 423–426.
34 D. Liu, Y. Xiang, X. Wu, Z. Zhang, L. Liu, L. Song, X. Zhao, S. Luo, W. Ma and J. Shen, *Nano Lett.*, 2006, **6**, 2375–2378.
35 A. Gorschinski, G. Khelashvili, D. Schild, W. Habicht, R. Brand, M. Ghafari, H. Bonnemann, E. Dinjus and S. Behrens, *J. Mater. Chem.*, 2009, **19**, 8829–8838.
36 C. S. Goonasekera, K. S. Jack, J. J. Cooper-White and L. Grondahl, *J. Mater. Chem. B*, 2013, **1**, 5842–5852.
37 A. M. Chong and X. Zhao, *J. Phys. Chem. B*, 2003, **107**, 12650–12657.
38 A. Arranz, C. Palacio, D. Garcia-Fresnadillo, G. Orellana, A. Navarro and E. Munoz, *Langmuir*, 2008, **24**, 8667–8671.
39 G. Tan, L. Zhang, C. Ning, X. Liu and J. Liao, *Thin Solid Films*, 2011, **519**, 4997–5001.
40 A. M. Schwartzberg, C. D. Grant, A. Wolcott, C. E. Talley, T. R. Huser, R. Bogomolni and J. Z. Zhang, *J. Phys. Chem. B*, 2004, **108**, 19191–19197.
41 H. Xu, J. Aizpurua, M. Käll and P. Apell, *Phys. Rev. E: Stat. Phys., Plasmas, Fluids, Relat. Interdiscip. Top.*, 2000, **62**, 4318.
42 M. Moskovits, *J. Raman Spectrosc.*, 2005, **36**, 485–496.
43 R. A. Alvarez-Puebla, D. S. Jr. dos Santos and R. F. Aroca, *Analyst*, 2007, **132**, 1210–1214.
44 T. Kiyonaga, Q. Jin, H. Kobayashi and H. Tada, *ChemPhysChem*, 2009, **10**, 2935–2938.

